Electromagnetic Inverse Profiling for Plasma Diagnostics via Sparse Recovery Approaches

Electromagnetic Inverse Profiling for Plasma Diagnostics via Sparse Recovery Approaches

Abstract— **The 1-D single-view multifrequency electromagnetic inverse scattering problem, or inverse profiling, is addressed to provide effective means for plasma diagnostics, taking into account the dispersive properties of such a medium. To this aim, first-order linearized approaches are considered in light of the renewed possibility to conveniently solve the underlying ill-posed problem through the sparse recovery optimization provided by the prominent compressive sensing theory. The intrinsic theoretical limitation of such a problem when tackled by means of the standard minimum energy solution is discussed, and effective approaches based on sparse recovery are proposed and tested against simulated data that deal with reliable benchmarks for microwave imaging in plasma diagnostics.**

Index Terms— **Compressive sensing (CS), electromagnetic inverse profiling, linear inverse scattering, microwave plasma diagnostics.**

I. Introduction

In microwave-induced plasma ion sources, noninvasive diagnostic methods based on microwave interferometry, time-domain spectroscopy and polarimetry are currently used to infer the mean value of plasma electron density over the line of sight along the propagation axis [1]–[4]. All the above methods provide line-averaged values of plasma electron density.

On the other hand, the actual profile of the plasma electron density is of great interest in studying plasma properties and can be retrieved by ultrafast reflectometry in principle [5], [6]. In this case, the probing-signal frequency can be varied to match the plasma frequency at which the total reflections occur; thus, by measuring the phase of the reflected signal, the position of the plasma surface can be inferred. However, a limit of such a technique is the impossibility to measure nonincreasing electron density plasma profiles due to the impenetrability of the first plasma layers [5], [6].

In this paper, we adopt relatively high-frequency probing with some advantages. First, at frequencies substantially higher than the cyclotron frequency, plasma constitutive relations are simpler since the plasma behaves as an isotropic medium. Second, by properly choosing the working frequency band well above the plasma frequency, plasmas behave as penetrable media, allowing for a volumetric diagnostic of their constitutive parameters. Finally, in small-sized plasma chambers with dimensions at a plasma frequency comparable to plasma wavelength, the use of short probing wavelengths mitigates the effect of multiple spurious reflections from the embedding case, without the need to model such cumbersome scenarios. As a result, the propagation of an electromagnetic wave in plasma can be addressed, to first approximation, as a 1-D problem in both large and compact reactors, such as tokamak and electron cyclotron resonance (ECR) ion source (ECRIS), respectively.

In light of the above-mentioned methods, 1-D inverse scattering techniques can represent a useful, noninvasive means to address plasma electron density profile measurement in plasma reactors. Pioneering works on the 1-D inverse scattering problem dates back two or three decades due to facing its computational simplicity and manageable mathematical modeling [7]–[13]. However, the main contributions have shown that the problem of recovering an embedded slab (processing multifrequency data) is severely limited both in terms of the amount of information (degree of freedom of the scattered field) and the spatial variations of the slabs, which can actually be retrieved [10], [11]. In particular, the retrieval problem is further deteriorated when the recovery problem is addressed with the homogeneous background, i.e., the "nondistorted" case [11], [13]. On the other hand, the approaches based on nonlinear recovery strategies entail the drawback of local minima [14]. For example, the Newton–Kantorovich-based approach proposed in [12] achieves satisfactory reconstructions only if the thickness of the inhomogeneous layer is assumed to be known (a strong *a priori* information), and noiseless measurements are considered. Therefore, the solution of the 1-D inverse scattering problem by standard minimum energy solutions implies severe intrinsic limitations, which, for real diagnostic applications, prevent exploiting its solution.

More recently, the compressive sensing (CS) framework offered the possibility to retrieve unknown signals by process-

This is the post-print of the following article: L. Di Donato, A. F. Morabito, G. Torrisi, T. Isernia, G. Sorbello, "Electromagnetic Inverse Profiling for Plasma Diagnostics via Sparse Recovery Approaches," IEEE Transactions on Plasma Science, vol. 47, n. 4, pp. 1781-1787, 2019.
Article has been published in final form at: https://ieeexplore.ieee.org/abstract/document/8668719 . DOI: 10.1109/TPS.2019.2902469.

ing a number of data at a sampling rate far below the well-known Nyquist rate, provided that the unknown can be represented in a sparse fashion [15]–[17]. This framework provides a great advantage in terms of number and kind of measurements needed to successfully perform both the measurements and the retrieval process. Finally, nearly optimal reconstruction and super-resolution can be achieved by means of sparse recovery approaches. According to the above reasoning, the 1-D electromagnetic inverse scattering problem is worth reconsidering since the CS-based approaches are able to recover different kinds of permittivity profiles, whose retrieval is forbidden via standard approaches based on minimum L^2-norm solutions [18]. As a result, an accurate solution of the 1-D inverse scattering problem can provide very useful information in plasma diagnostics.

According to the above reasoning, in this paper, we investigate the possibility to retrieve unknown 1-D dispersive lossy plasma profiles processing multifrequency scattered (i.e., reflected) field data.

The paper is structured as follows. In Section II, the imaging problem is formulated, and the linearized approaches under the Born approximation (BA) and Rytov approximation (RA) are recalled. In Section III, the adopted sparse solution approaches are introduced and described in the case of multifrequency data processing, while Section IV is concerned with the method validation against the simulated data in the case concerned with cold lossy dispersive plasma media. The conclusions follow. Throughout the paper, the time factor $\exp\{j\omega t\}$ is assumed and dropped.

II. Statement of the Problem

A. Integral Formulation and Linearized Inversion Models

We consider the 1-D inverse scattering problem wherein the unknown slab is embedded into a homogeneous domain with complex dielectric permittivity ε_b in the range $[-L/2, L/2]$ over the z-direction assumed as propagation axis, i.e., the line of sight in plasma chambers. The probing field, i.e., the field in absence of the slab, is assumed plane waves of unitary amplitude $E_i(z,\omega) = \exp(-\jmath k_z z)$ propagating in z-direction at difference frequencies, and the scattered field is measured at positions $z^- \leq -L/2$ outside the investigation domain. Here, $k_z = \omega(\mu_0\varepsilon_0\varepsilon_b)^{(1/2)}$ is the propagation constant with $\varepsilon_b = \varepsilon_b' - j\sigma_b/\omega\epsilon_0$ being the equivalent permittivity accounting for both the displacement and conductivity currents in the background medium. Under the above-mentioned assumptions, the incident field (i.e., the field without the slab) and the total field (i.e., the field in presence of the slab) must satisfy the following Helmholtz equations, respectively:

$$\frac{\partial^2 E_i}{\partial z^2} + k_z^2 E_i = 0 \tag{1}$$

$$\frac{\partial^2 E}{\partial z^2} + k^2(z) E = 0. \tag{2}$$

Defining the scattered field as $E_s = E - E_i$ and subtracting (1) from (2), one easily obtains the nonhomogeneous Helmholtz equation for the scattered field

$$\frac{\partial^2 E_s}{\partial z^2} + k_z^2 E_s = -k_z^2 \chi(z)\ E. \tag{3}$$

For any arbitrary ω, (3) can be solved through the electromagnetic potentials theory [7], and the inverse scattering problem can be conveniently formulated as the solution to the following two coupled integral equations:

$$E(z,\omega) = E_i(z,\omega) + k_z^2 \int_{-\frac{L}{2}}^{\frac{L}{2}} g_i(z,z',\omega) E(z',\omega)\chi(z',\omega) dz' \qquad \omega \in \Omega,\ z \in [-L/2, L/2] \tag{4}$$

$$E_s(z^-,\omega) = k_z^2 \int_{-\frac{L}{2}}^{\frac{L}{2}} g_e(z^-,z',\omega) E(z',\omega)\chi(z',\omega) dz' \qquad \omega \in \Omega,\ |z^-| \geq L/2. \tag{5}$$

In (4) and (5), the respective Green's functions can be expressed as

$$g_i(z,z',\omega) = -\frac{j}{2k_z}\exp\big(-jk_z|z'-z|\big) \tag{6}$$

$$g_e(z^-,z',\omega) = -\frac{j}{2k_z}\exp\big(-jk_z|z'-z^-|\big) \tag{7}$$

while the contrast function, i.e., the actual unknown, relating the dielectric properties of the slab to those of the background medium, can be ultimately expressed as

$$\chi(z,\omega) = \frac{\varepsilon_p(z,\omega)}{\varepsilon_b(\omega)} - 1. \tag{8}$$

In (8), ε_p is the complex permittivity of the (unknown) plasma slab. Moreover, $\Omega = [\omega_1, ..., \omega_m, ..., \omega_M]$ is the discrete set of probing angular frequencies used to gather field data.

The solution to (4) and (5) implies a nonlinear problem since the total field within the domain is unknown, depending on the turns in the contrast function. A possibly very simple way to circumvent this drawback is resorting to the first-order models [8], [11], [13], [19], [20], such as the BA and RA. Both approximations are valid when the slab is weak, i.e., when it has dielectric properties similar to those of the background medium. In particular, the BA simply requests to substitute the total field in (4) with the incident one, while the RA needs to account for the time delay the field accumulates when it propagates into an electrically extended medium, even of small contrast. As a result, the BA produces better estimates of a slab with large deviations in the refractive index but small size, while the RA provides more accurate estimates for electrically extended slabs with small deviations in the refractive index [21].

The recovery problem (4) and (5) has been studied mainly under the BA approximation. For example, in [9], a quadratic approach based on a field approximation given by the truncation of the geometrical Born–Neumann series at the first-order term has been proposed. It has been shown that only low-harmonics content profiles can be effectively retrieved. On the other hand, the so-called "distorted Born" case has been addressed in [11] and [10], where the ultimately achievable imaging performance has been analytically investigated. In such a case, the number of independent parameters and the "spatial harmonic content" that can be retrieved form inversion of multifrequency scattered field data stays very low and, in addition, is limited to the class of slowly varying contrasts. As a result, several kinds of profiles that can be of actual interest in inverse profiling applications, such as step-wise rectangular slab or similar, cannot be retrieved at all.

B. Dispersive Model for Cold Isotropic Lossy Plasma

As we are interested in inverse profiling of a dispersive medium, whose real and imaginary parts of the permittivity are frequency dependent, the data equation has to be slightly manipulated through simple algebra in order to express the unknown contrast function in terms of quantities that do not depend on frequency. We start considering the explicit frequency dependence of the permittivity for an isotropic (unmagnetized) cold plasma with electronic collisions as follows:

$$\varepsilon_p = 1 - \frac{\omega_p^2}{\omega^2 + \nu^2} - j\frac{\omega_p^2 \nu}{\omega(\omega^2 + \nu^2)}. \tag{9}$$

Thus, the plasma conductivity becomes

$$\sigma_p = \frac{\epsilon_0 \nu \omega_p^2}{\omega^2 + \nu^2}.$$

For a vacuum background, i.e., $\varepsilon_b = 1$ and $\sigma_b = 0$, the contrast function reads

$$\chi(z, \omega) = -\frac{\omega_p^2}{\omega^2 + \nu^2} - j\frac{\omega_p^2 \nu}{\omega(\omega^2 + \nu^2)}.$$

Therefore, under the reasonable assumption $\omega^2 >> \nu^2$ (i.e., at sufficiently high probing frequency with respect to the collision frequency), the data equation (5) can be recast in terms of the unknowns ω_p^2 and ν, that is,

$$\hat{E}_s(z^-, \omega) = \hat{M}\, k_z^2 \int_{-L/2}^{L/2} g_e(z^-, z', \omega) E_i(z', \omega) \times \left(-\frac{\omega_M^2}{\omega^2}\frac{\omega_p^2(z')}{\omega_M^2} - j\frac{\omega_M^3}{\omega^3}\frac{\nu(z')\omega_p^2(z')}{\omega_M^3} \right) dz' \tag{10}$$

with

$$\hat{E}_s = \begin{cases} E_s(z^-) \\ \dfrac{E_s(z^-)}{E_i(z^-)} \end{cases} \qquad \hat{M} = \begin{cases} 1 \\ \dfrac{1}{E_i(z^-)} \end{cases} \tag{11}$$

for BA (top row) and RA (bottom row), respectively. Moreover, in (10), it is convenient to introduce the normalization factors ω_M^2 and ω_M^3. In this way, the data equation can be expressed in matrix–vector form involving only frequency independent real quantities as follows:

$$\begin{bmatrix} -\dfrac{\omega_M^2}{\omega^2}\mathcal{R}e(\mathcal{S}) & \dfrac{\omega_M^3}{\omega^3}\mathcal{I}m(\mathcal{S}) \\ -\dfrac{\omega_M^2}{\omega^2}\mathcal{I}m(\mathcal{S}) & -\dfrac{\omega_M^3}{\omega^3}\mathcal{R}e(\mathcal{S}) \end{bmatrix} \begin{bmatrix} \dfrac{\omega_p^2}{\omega_M^2} \\ \dfrac{\nu\omega_p^2}{\omega_M^3} \end{bmatrix} = \begin{bmatrix} \mathcal{R}e(\hat{E}_s) \\ \mathcal{I}m(\hat{E}_s) \end{bmatrix} \tag{12}$$

where $\mathcal{R}e(S)$ and $\mathcal{I}m(S)$ are the real and imaginary parts, respectively, of the integral operator kernel in (10).

C. Two-Step Inversion Strategy

The problem (12), which consists of a set of linear equations in the unknowns ω_p^2 and the product $\nu\omega_p^2$, could be principally and directly solved by means of numerical approaches based on the minimum energy solution in the space of square integrable functions, such as the truncated singular value decomposition (TSVD) or Tikhonov regularization [18]. However, as discussed in Section I and as will be shown in Section IV, the standard energy minimum solution is intrinsically unable to provide satisfactory reconstructions for a large class of unknown profiles. Furthermore, due to the way the two actual unknowns appear in the data equation, i.e., through their product in the imaginary part, we propose a two-step inversion strategy.

Since the order of collision frequency is assumed to be $\nu << \omega_M$, we can reasonably assume that the impact of the collision frequency on the scattered field is negligible. As a result, the problem can be split in two subproblems, wherein the first part is concerned with the recovery of ω_p^2 solving the first N_M equations of the system (12). Afterward, the remaining part of the system can be solved for ν. The first subproblem reads

$$\begin{bmatrix} -\dfrac{\omega_M^2}{\omega^2} & \mathcal{R}e(\mathcal{S}) \\ -\dfrac{\omega_M^2}{\omega^2} & \mathcal{I}m(\mathcal{S}) \end{bmatrix} \begin{bmatrix} \dfrac{\omega_p^2}{\omega_M^2} \end{bmatrix} = \begin{bmatrix} \mathcal{R}e(\hat{E}_s) \\ \mathcal{I}m(\hat{E}_s) \end{bmatrix}. \tag{13}$$

Once the vector ω_p^2 is retrieved, its estimated value can be put into the rest of the linear system to solve the subproblem

$$\begin{bmatrix} \dfrac{\omega_M}{\omega^3}\omega_p^2 & \mathcal{I}m(\mathcal{S}) \\ -\dfrac{\omega_M}{\omega^3}\omega_p^2 & \mathcal{R}e(\mathcal{S}) \end{bmatrix} \begin{bmatrix} \dfrac{\nu_p}{\omega_M} \end{bmatrix} = \begin{bmatrix} \mathcal{R}e(\hat{E}_s) - a \\ \mathcal{I}m(\hat{E}_s) - b \end{bmatrix}. \tag{14}$$

Here, a and b are defined by means of the matrix–vector inner product

$$a = \left[-\frac{\omega_M^2}{\omega^2}\mathcal{R}e(\mathcal{S}) \right] \left[\frac{\omega_p^2}{\omega_M^2} \right] \tag{15}$$

$$b = \left[-\frac{\omega_M^2}{\omega^2}\mathcal{I}m(\mathcal{S}) \right] \left[\frac{\omega_p^2}{\omega_M^2} \right]. \tag{16}$$

III. Sparse Solution Approaches for Rectangular Slabs

CS theory [16], [17] provides several optimization tools based on constrained ℓ_1 minimization, provided that the unknown signal can be represented through a sparse basis [15]. In the following, the basics are briefly recalled.

Let us consider a generic linear problem of the following kind:

$$\Theta x = y \tag{17}$$

where y is the $N_M \times 1$ data vector, x is the $N_z \times 1$ unknown vector, and Θ is the $N_M \times N_z$ matrix, which relates the unknown to data vector, also known as sensing matrix.

Let us also adopt a convenient representation matrix Ψ such that $x = \Psi s$ with only few coefficients s different from zero. According to CS theory, it is possible to solve the inverse problem (17) even if N_M is (much) less than N_z but is sufficiently larger than the number K of coefficients different from zero (with $K < N_M < N_z$). In this respect, a rule of thumb assumes that the number of measurements needed to achieve a reliable solution is $N_M \geq cK \log(N_z/K)$, with c as a small constant [17].

Furthermore, additional properties also have to be satisfied to reliably apply CS-based approaches. In particular, the matrix $A = \Theta\Psi$ should not cancel out any information about the original signal, i.e., the image of the rows of Θ should be

spread out in the space defined by the columns of Ψ, and vice versa. Accordingly, the larger the incoherence is, the better the probability to retrieve sparse signals by compressed measurements. Moreover, a related property states that matrix A should approximately preserve the Euclidean length of K-sparse signals, so that each K-sparse vector has to show a nonnegligible image in that data space. The exact requirements of the latter property is formalized by means of the so-called restricted isometry property [16], [17], which guarantees conditions for a nearly exact recovery. By leaving aside the proof of these properties for matrix A (which generally can be verified for random Gaussian matrices), it is only worth to recall that, in the linearized inverse scattering problem, the functional relationship between data and unknown is ruled by the Fourier transform [7], [18]. Numerical analysis of canonical cases has suggested successful reconstructions in more than 50% of cases when $N_M \geq 4K$ and in more than 90% of cases when $N_M \geq 8K$ [16], [17].

Provided the above hypotheses holds true, it is possible to solve the inverse linear problem $As = y$ by means of different optimization constrained problems [16], [17] based on minimization of the ℓ_1-norm of the unknown when represented in a sparse dictionary [22]. Moreover, recent works have shown that ℓ_1-optimization can also be exploited if the objective function involves the directional derivative of the unknown [23]. For these reasons, we consider the following recovery problems:

$$\text{argmin } \|s\|_{\ell_1} \quad \text{subject to} \quad \|As - y\|_{\ell_2} \leq \delta \tag{18}$$

$$\text{argmin } \left\| \frac{ds}{dz} \right\|_{\ell_1} \quad \text{subject to} \quad \|As - y\|_{\ell_2} \leq \delta \tag{19}$$

and the dual version of (19) as follows:

$$\text{argmin } \|As - y\|_{\ell_2} \quad \text{subject to} \quad \left\| \frac{ds}{dz} \right\|_{\ell_1} \leq \epsilon \tag{20}$$

In (18), s is the unknown vector, $\|\cdot\|_{\ell_1}$ and $\|\cdot\|_{\ell_2}$ denote the ℓ_1-norm and ℓ_2-norm, respectively, and the parameter δ, which depends on the level of required accuracy as well as on the modeling (field approximation) and measurement error (noise on data), is positive. It is worth noting that the choice of δ is not a simple task; however, in order to avoid the null vector solution, δ can be chosen as a tradeoff between the reconstruction accuracy and the feasibility of the optimization task, i.e., $1/10||y||_{\ell_2} \leq \delta \leq ||y||_{\ell_2}$. Similar considerations apply to the choice of the parameter ϵ in (20), which also depends on the sparsity of the unknown at hand. Moreover, taking into account the real positive valued unknowns, a further positivity constraint ($s \geq 0$) has been enforced in (18), (19) and (20).

The approach (18) is known as basis pursuit denoising or least absolute shrinkage and selection operator problem [17]. In (18), the minimization of the ℓ_1-norm promotes the search of sparse solutions, while the constraint enforces data consistency, i.e, among all the solutions consistent with the measured data (within the given error δ), the sparsest one is sought.

On the other hand, in (19) and (20), the minimization of the ℓ_1-norm promotes the search of solutions with a sparse derivative among all the solutions consistent with the measured data (within the given error threshold δ). In Section IV, the adoption of the different inversion strategies is shown to be assessed on the basis of the sought plasma dielectric profile.

It is worth noting that the optimization problems introduced above will be applied separately in two subsequent steps to solve the systems (13) and (14), respectively. Since the regularization parameters may not be the same value, we refer to them with subscripts 1 (δ_1 or ϵ_1) and 2 (δ_2 or ϵ_2) to distinguish between the first and second optimization steps.

Finally, it is worth mentioning that, for all the numerical examples in the following section, we have considered only the usual pixel representation basis (pulsewidth). This occurs because, although more refined representation bases could be in principle adopted, the very small number of independent parameters brought by the measurement process in the 1-D inverse scattering problem would require expansion bases able to represent the unknown profile with a very low number of nonnull coefficients, i.e., large "degree of sparsity" (small K). As an example, wavelet representation bases, thus far exploited in the framework of inverse scattering, are generally not suitable to guarantee such a condition.

IV. Numerical Examples

We consider several examples dealing with the recovery of plasma slabs with different shapes, dimensions, and constitutive parameters. In all the numerical setups, the length of the investigation domain is $L = 26$ cm, which is a typical length of a ECRIS plasma chamber operating at the plasma-heating frequency $f_{RF} = \omega_{RF}/2\pi = 2.45$ GHz. The domain is probed by means of a set of plane waves at different angular frequencies in the band $[18.5 - 26.5]$ GHz (being the probing signal-frequencies $\omega_m \gg \omega_{RF}$) with a step of 100 MHz. This frequency range has been used, for example, in [1], where a frequency-swept-based microwave interferometry has allowed for the noninvasive measurement of electron plasma density in an ECRIS-type device. The scattered field is measured at $z^- = -L/2 = -13$ cm. The reconstruction performance has been evaluated by the standard error metrics defined by the following:

$$err_{\omega_p^2} = \frac{||\omega_p^2 - \hat{\omega}_p^2||^2}{||\omega_p^2||^2} \tag{21}$$

$$err_{\nu} = \frac{||\nu - \hat{\nu}||^2}{||\nu||^2} \tag{22}$$

where the quantities under the hat symbol $\hat{}$ are the reconstructed values.

Different plasma profiles have been considered taking into account the typical measured electron density profiles of plasma ion sources, with the exception of the first case that represents only an initial check aimed to show peculiar properties of the adopted inverse profiling approach based on CS.

The first property is a lossless (i.e., collisionless), very thin rectangular plasma slab of 5 mm with a sparsity degree of $K = 5$ (i.e., the number of nonnull expansion coefficients in the 1-D pixel basis). At the smallest probing wavelength (1.13 cm), the dimension of the slab is under the Rayleigh limit of the diffraction tomography ($\lambda/2$). In all the frequency bands, $|\chi| \leq 0.01$; thus, the BA is fully satisfied over all the whole frequency range. The reflected fields have been simulated by means of an in-house method-of-moment (MoM) forward simulator based on a conjugate gradient minimization scheme in which the exact permittivity plasma formula (9) (without the approximation $\nu^2 << \omega^2$) has been considered. Finally, the scattered field has been corrupted with an additive white Gaussian noise of 5%. We have first considered the

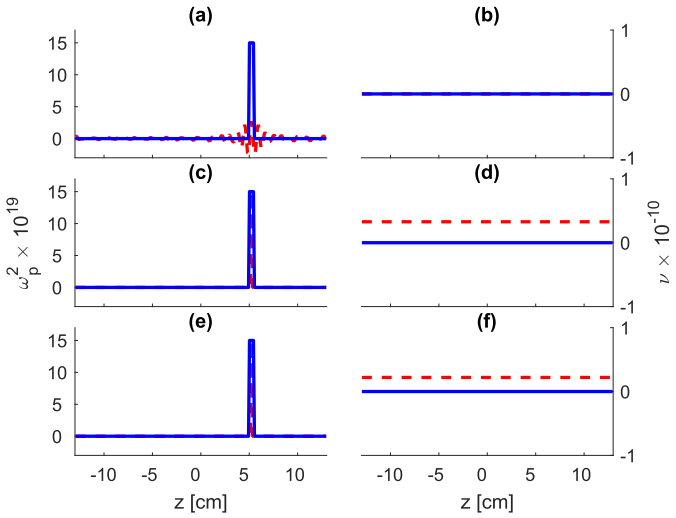

Fig. 1. Reconstruction of a thin lossless (collisionless) plasma pulselike slab by means of BA setting. (a) Plasma frequency and (b) collision frequency retrieved by means of TSVD (considering only the first largest 32 singular values), $err_{\omega_p^2} = 94\%$. Reconstruction of the plasma frequency and collision frequency by means of the ℓ_1-based approach (18). (c) and (d) Considering all the 81 measurements ($\delta_{1,2} = 0.03$). (e) and (f) Considering only 2 randomly chosen measurements at 20 and 24.2 GHz ($\delta_{1,2} = 0.0045$). In both cases, the reconstruction error is about $err_{\omega_p^2} = 80\%$. Blue solid line: actual profile. Red dashed line: retrieved profile.

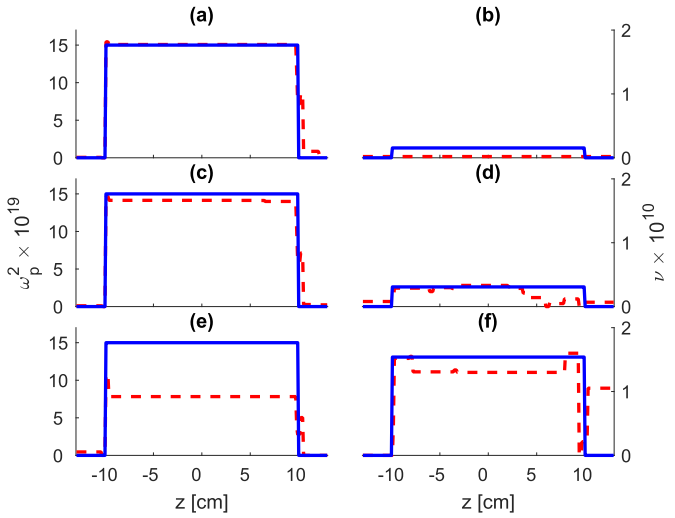

Fig. 2. Reconstruction of lossy tick plasma rectangular slabs with different peak values of collision frequency via RA by means of CS approach (19). Plasma frequency (left column) and collision frequency (right column) retrieved for (a) and (b) $\delta_{1,2} = 0.005$, $err_{\omega_p^2} = 0.94\%$, and $err_\nu = 76.91\%$; (c) and (d) $\delta_1 = 0.005$ and $\delta_2 = 0.0045$, $err_{\omega_p^2} = 10.9\%$, and $err_\nu = 18.15\%$; (e) and (f) $\delta_1 = 0.0075$ and $\delta_2 = 0.0057$, $err_{\omega_p^2} = 23.27\%$, and $err_\nu = 11.77\%$. Blue solid line: actual profile. Red dashed line: retrieved profile.

standard reconstruction approaches based on the singular value decomposition (SVD). The inversion is performed through the TSVD [18] considering only the first singular values larger than 20 dB with respect to the maximum one. The results are shown in Fig. 1(a)–(b). On the other hand, the reconstruction obtained with approach (18) is shown in Fig. 1(c)–(d). As it can be seen, the sparsity-based approach is able to recover the real part of the plasma frequency fairly well, considering that the retrieved collision frequency profile is negligible, while the standard minimum energy approach is completely unable to retrieve the plasma pulsation profile. The CS-based approach is able to estimate the position and shape, even if the width of the slab is underestimated such that only one of the actual five coefficients is retrieved. Additional details of the reconstruction processes and performance are reported in the caption of Fig. 1. In this respect, the minimum nonredundant number of complex samples needed to represent the scattered field (degrees of freedom), according to [11, eq. 13], stays very low at $\simeq 0.3$. For this reason, it is very challenging to recover exactly a pulselike rectangular slab from such a limited amount of information, even when adopting sparsity promoting approaches. However, the reconstruction capabilities are unaltered even if the number of processed measurements are massively reduced to only two of the recorded set that are randomly chosen among all the available measurements, as shown in Figs. 1(e)–(f). Finally, although the reconstruction errors are large in all the considered cases (see error values reported in the caption of Fig. 1), the sparsity recovery approach allows for the appraisal of the magnitude of the plasma frequency, while the TSVD reconstruction brings completely unsatisfactory results.

The second set of examples considers the same simulation parameters but for slabs of different width (L_{slab}=20 cm), which may resemble a realistic electron density profile. Usually, an almost flat high-density plasma is formed inside the ECR "plasmoid" delimited by the ECR layer, where the confinement of the magnetic field B (having the a so-called "minimum B structure") satisfies the ECR condition $B_{ECR} = 2\pi f_{RF} m_e/e$. The electron density is peaked on the plasma cavity axis inside the "plasmoid," while it decreases very fast outside the ECR zone [24]. In this case, taking into account the wider extension of the plasma, the dimension of the slab is long, with several wavelengths in the whole adopted frequency range ($12 < L_{\text{slab}}/\lambda < 18$). For this reason, the RA has been considered in approach (19), as the approach (18) is expected to be unsuccessful.

Three different collision frequency values were chosen to take into account both the linearized model approximation and the sensitivity of the inversion approach. Indeed, the adopted models cannot take into account plasma collision frequency values that do not fulfill condition $\nu^2 << \omega^2$. On the other hand, too small collision frequency values entail decreasing losses, which are very difficult to retrieve when on the order of the model approximation and measurement errors. In this case, the number of degrees of freedom of the scattered field (calculated via [11, eq. 13]) is 10, so that more reliable reconstructions are expected with respect to the thin slab. In addition, in this case, the superior performance of the sparsity promoting approach is confirmed with respect to the TSVD approach. The results obtained in the latter resembles those previously shown for the thin slab and are not shown for the sake of brevity. This method achieves very small final reconstruction errors of approximately 0.4% for the plasma frequency profile, as shown in Fig. 2. On the other hand, taking into account the above reasoning, reconstructions for the collision frequency become better for increasing values of ν, as shown in Fig. 2 (b), (d), and (f) ($0.1\omega_{RF}$, $0.2\omega_{RF}$, and ω_{RF} for the peak value of ν, respectively, at $f_{RF} = 2.45$ GHz). In particular, for the greater value of ν, the approach is able to

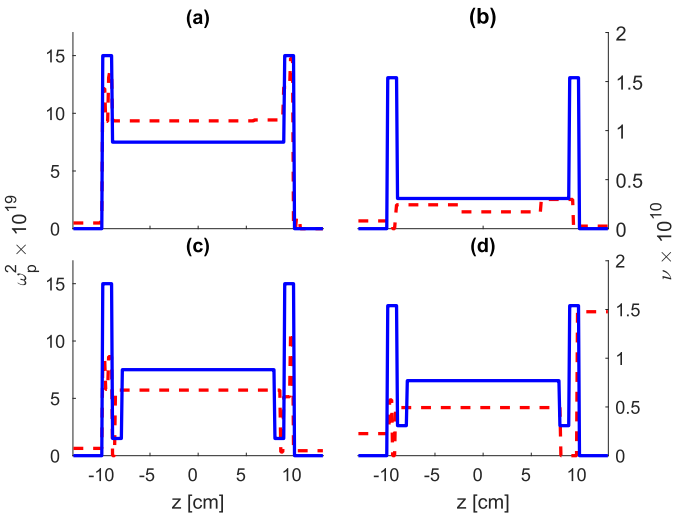

Fig. 3. Reconstruction of a tick "horn"-shaped lossy plasma slab via RA and approach (20). (a) Plasma frequency and (b) collision frequency retrieved for $\epsilon_1 = 16$ and $\epsilon_2 = 50$, $err_{\omega_p^2} = 7.24\%$, and $err_\nu = 68\%$. Reconstruction of a thick "double-horn"-shaped lossy plasma slab via RA and approach (20). (c) Plasma frequency and (d) collision frequency retrieved for $\epsilon_1 = 19$ and $\epsilon_2 = 200$, $err_{\omega_{p2}} = 16.29\%$, and $err_\nu = 80.89\%$. Blue solid line: actual profile. Red dashed line: retrieved profile.

achieve coarse reconstruction of the central part of the collision frequency profile, while it slightly underestimates the value of the plasma frequency, as shown in Fig. 2(e) and (f).

Finally, we have considered more complicated stepwise shaped plasma slabs in order to assess the capability of the proposed approach in retrieving slabs with a smaller degree of sparsity (larger K) as well as with more realistic plasma profiles. In this case, we consider a "hole" in the distribution of the electron density with two peaks almost exclusively at the ECR zones, i.e., a hollow density profile. The electron energy peaks can sometimes be seen just outside the RF resonances, and a hot electron ring can sometimes be seen outside the core of an ECR ion source [24]. However, in this case, the approach exploited to perform inverse profiling is (20), since the number of nonnull derivative coefficients is larger than the rectangular slab. Therefore, this approach is expected to show better performance than (19), which has been confirmed by a number of extensive numerical trials.

As shown in Fig. 3, the proposed approach is still capable of retrieving the shape of the slab but with larger reconstruction error cost. However, the shape of the plasma pulsation profile can be effectively inferred form the achieved results. Indeed, the number of degrees of freedom are essentially related to the extent of the slab (for any given frequency band); thus, the reconstruction performance is expected to worsen with increasing number of null unknown coefficients even in the stepwise representation basis.

Finally, it is interesting to observe that in the case of thick slabs, when the number of processed data is gradually reduced at different undersampling rates, the reconstruction is unsatisfactory both from a qualitative and quantitative points of view, opposite to what happens in the case of pulse-like plasma slabs (results not shown for the sake of brevity). This is in agreement with the results and the argumentation shown in the case of thin slab, where instead the reconstruction capability is essentially independent of the number of processed data.

V. Conclusion

The problem of retrieving 1-D isotropic unmagnetized dispersive plasma profiles from multifrequency reflected waves has been addressed via CS linearized-based approaches. This allows for achieving reconstructions that cannot be addressed by means of standard minimum energy solution approaches, such as the SVD and the Tikhonov regularization. In particular, sparsity-promoting approaches are able to estimate realistic plasma pulsation profiles with good accuracy as well as collision frequency profiles when the latter are not smaller than one order of magnitude of the probing frequencies. On the other hand, for more complicated stepwise constant representation of plasma slabs, the performance of the methods tends to worsen because of the limited amount of information content that can be gathered from 1-D multifrequency scattering experiments. This research will be further addressed in processing data gathered under experimental conditions dealing with ECRIS chambers, as well as in adopting different inversion approaches and representations that are able to take full advantage of sparsity based approaches.

VI. Acknowledgments

The authors would to thank Dr. Celona and Dr. Mascali of Laboratori Nazionali del Sud, Istituto Nazionale di Fisica Nucleare, Catania, Italy, for their fruitful suggestions about plasma fusion devices and plasma diagnostics techniques' overview.

References

[1] D. Mascali *et al.*, "The first measurement of plasma density in an ECRIS-like device by means of a frequency-sweep microwave interferometer," *Rev. Sci. Instrum.*, vol. 87, no. 9, 2016, Art. no. 095109.

[2] G. Torrisi *et al.*, "Microwave frequency sweep interferometer for plasma density measurements in ECR ion sources: Design and preliminary results," *Rev. Sci. Instrum.*, vol. 87, no. 2, 2016, Art. no. 02B909.

[3] S. M. Meier, T. V. Tsankov, D. Luggenhölscher, and U. Czarnetzki, "Measurement of plasma densities by dual frequency multichannel boxcar THz time domain spectroscopy," *J. Phys. D, Appl. Phys.*, vol. 50, no. 24, 2017, Art. no. 245202.

[4] G. Torrisi *et al.*, "A new interferometric/polarimetric setup for plasma density measurements in compact microwave-based ion sources," *J. Instrum.*, vol. 12, no. 10, 2017, Art. no. C10003.

[5] F. Simonet, "Measurement of electron density profile by microwave reflectometry on tokamaks," *Rev. Sci. Instrum.*, vol. 56, no. 5, pp. 664–669, Feb. 1985.

[6] D. E. Aguiam *et al.*, "Estimation of X-mode reflectometry first fringe frequency using neural networks," *IEEE Trans. Plasma Sci.*, vol. 46, no. 5, pp. 1323–1330, May 2018.

[7] K. I. Hopcraft and P. R. Smith, *An Introduction to Electromagnetic Inverse Scattering*, vol. 7. Springer, 2013.

[8] A. G. Tijhuis, "Born-type reconstruction of material parameters of an inhomogeneous, lossy dielectric slab from reflected-field data," *Wave Motion*, vol. 11, no. 2, pp. 151–173, 1989.

[9] A. Brancaccio, V. Pascazio, and R. Pierri, "A quadratic model for inverse profiling: The one-dimensional case," *J. Electromagn. Waves Appl.*, vol. 9, nos. 5–6, pp. 673–696, 1995.

[10] R. Pierri, A. Brancaccio, G. Leone, and F. Soldovieri, "Electromagnetic prospection via homogeneous and inhomogeneous plane waves: The case of an embedded slab," *AEU-Int. J. Electron. Commun.*, vol. 56, no. 1, pp. 11–18, 2002.

[11] R. Pierri, R. Persico, and R. Bernini, "Information content of the Born field scattered by an embedded slab: Multifrequency, multiview, and multifrequency–multiview cases," *J. Opt. Soc. Amer. A, Opt. Image Sci.*, vol. 16, no. 10, pp. 2392–2399, 1999.

[12] V. A. Mikhnev and P. Vainikainen, "Two-step inverse scattering method for one-dimensional permittivity profiles," *IEEE Trans. Antennas Propag.*, vol. 48, no. 2, pp. 293–298, Feb. 2000.

[13] R. Persico and F. Soldovieri, "One-dimensional inverse scattering with a Born model in a three-layered medium," *J. Opt. Soc. Amer. A, Opt. Image Sci.*, vol. 21, no. 1, pp. 35–45, 2004.

[14] T. Isernia, V. Pascazio, and R. Pierri, "On the local minima in a tomographic imaging technique," *IEEE Trans. Geosci. Remote Sens.*, vol. 39, no. 7, pp. 1596–1607, Jul. 2001.
[15] E. J. Candès, M. B. Wakin, and S. P. Boyd, "Enhancing sparsity by reweighted ℓ_1 minimization," *J. Fourier Anal. Appl.*, vol. 14, nos. 5–6, pp. 877–905, 2008.
[16] D. L. Donoho, "Compressed sensing," *IEEE Trans. Inf. Theory*, vol. 52, no. 4, pp. 1289–1306, Apr. 2006.
[17] R. G. Baraniuk, "Compressive sensing [lecture notes]," *IEEE Signal Process. Mag.*, vol. 24, no. 4, pp. 118–121, Jul. 2007.
[18] M. Bertero and P. Boccacci, *Introduction to Inverse Problems in Imaging*. Bristol, U.K.: Institute of Physics, 1998.
[19] L. Di Donato, R. Palmeri, G. Sorbello, T. Isernia, and L. Crocco, "Assessing the capabilities of a new linear inversion method for quantitative microwave imaging," *Int. J. Antennas Propag.*, vol. 2015, Jun. 2015, Art. no. 403760.
[20] L. Di Donato, R. Palmeri, G. Sorbello, T. Isernia, and L. Crocco, "A new linear distorted-wave inversion method for microwave imaging via virtual experiments," *IEEE Trans. Microw. Theory Techn.*, vol. 64, no. 8, pp. 2478–2488, Aug. 2016.
[21] M. Slaney, A. C. Kak, and L. E. Larsen, "Limitations of imaging with first-order diffraction tomography," *IEEE Trans. Microw. Theory Techn.*, vol. 32, no. 8, pp. 860–874, Aug. 1984.
[22] N. Anselmi, M. Salucci, G. Oliveri, and A. Massa, "Wavelet-based compressive imaging of sparse targets," *IEEE Trans. Antennas Propag.*, vol. 63, no. 11, pp. 4889–4900, Nov. 2015.
[23] M. T. Bevacqua, L. Crocco, L. Di Donato, and T. Isernia, "Microwave imaging of nonweak targets via compressive sensing and virtual experiments," *IEEE Antennas Wireless Propag. Lett.*, vol. 14, pp. 1035–1038, 2014.
[24] G. Torrisi *et al.*, "Full-wave FEM simulations of electromagnetic waves in strongly magnetized non-homogeneous plasma," *J. Electromagn. Waves Appl.*, vol. 28, no. 9, pp. 1085–1099, 2014.